Pressure- and flow-driven biomechanical factors associate with carotid atherosclerosis assessed by computed tomography angiography

Tziotziou, Aikaterini; Liu, Yanjing; Fontana, Federica; Bierens, Juul; Nederkoorn, Paul J.; de Jong, Pim A.; Kooi, M. Eline; Mess, Werner; van der Lugt, Aad; van der Steen, Antonius F.W.

DOI
10.1016/j.atherosclerosis.2025.120415

Publication date
2025

Document Version
Final published version

Published in
Atherosclerosis

Atherosclerosis 408 (2025) 120415

Contents lists available at ScienceDirect

Atherosclerosis

journal homepage: www.elsevier.com/locate/atherosclerosis

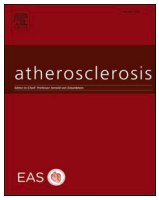

Pressure- and flow-driven biomechanical factors associate with carotid atherosclerosis assessed by computed tomography angiography

Aikaterini Tziotziou [a,b], Yanjing Liu [a], Federica Fontana [c], Juul Bierens [d], Paul J. Nederkoorn [e], Pim A. de Jong [f], M. Eline Kooi [d], Werner Mess [d], Aad van der Lugt [b], Antonius F.W. van der Steen [a], Daniel Bos [b,g], Jolanda J. Wentzel [a], Ali C. Akyildiz [a,c,*]

[a] Department of Cardiology, Biomedical Engineering, Cardiovascular Institute, Thorax Center, Erasmus MC, Rotterdam, the Netherlands
[b] Department of Radiology & Nuclear Medicine, Erasmus Medical Center, Rotterdam, the Netherlands
[c] Department of Biomechanical Engineering, Delft University of Technology, Delft, the Netherlands
[d] Department of Radiology and Nuclear Medicine, CARIM Cardiovascular Research Institute Maastricht, Maastricht University Medical Center (MUMC+), Maastricht, the Netherlands
[e] Department of Neurology, University Medical Center Amsterdam, Amsterdam, the Netherlands
[f] Department of Radiology, University Medical Center Utrecht and Utrecht University, Utrecht, the Netherlands
[g] Department of Epidemiology, Erasmus Medical Center, Rotterdam, the Netherlands

ARTICLE INFO

Keywords:
Atherosclerosis
Carotid artery
calcification
Computed tomography angiography
Mechanical stress
Shear stress
Oscillatory shear index

ABSTRACT

Background and aims: Local biomechanical factors are known to influence atherosclerosis in extracranial carotid arteries. While the role of some flow-driven biomechanical factors has been investigated, the influence of pressure-driven mechanical wall stress (MWS) has received limited attention. In this study, the association of the pressure-driven and flow-driven biomechanical factors with carotid atherosclerosis was examined.
Methods: Carotid arteries (n = 150) with mild-to-moderate stenosis from 75 symptomatic patients (Plaque-At-Risk study) were imaged using multi-detector computed tomography angiography (MDCTA) at the time of inclusion and after 2 years. Structural changes in carotid wall and calcifications were quantified from MDCTA data while the local baseline biomechanical factors in the carotids were determined using fluid-structure interaction (FSI) computational models. The associations of the local pressure-driven and flow-driven biomechanical factors with the carotid wall and calcification changes were studied using Generalized Linear Mixed models.
Results: Over two years, plaque sectors, with calcified and non-calcified sectors combined, exhibited minimal change in wall thickness, likely due to medical treatment. High MWS was associated ($p < 0.001$) with a reduction in plaque thickness. In calcified plaque sectors, high MWS and low oscillatory shear index (OSI) were associated ($p < 0.001$) with greater calcification thickness increase. The distance between the lumen and calcification decreased over time, especially in the sectors exposed to high time-averaged wall shear stress (TAWSS) and high MWS.
Conclusions: Our results suggest that the pressure-driven local MWS and flow-driven OSI and TAWSS significantly correlate with the development of calcified and non-calcified plaques in carotid arteries.
Registration: URL: https://www.clinicaltrials.gov; Unique identifier: NCT01208025.

1. Introduction

One of the key indicators of risk for ischemic events is carotid artery atherosclerosis [1]. The uneven distribution of atherosclerotic plaques in vascular territories and the variation in their compositions suggest the influence of local risk factors [2,3]. A key player in the initiation, development, and compositional changes of atherosclerotic plaques is local artery biomechanics [4,5].

Previously, some blood flow-driven biomechanical factors were shown to correlate with atherosclerosis [6]. For instance, atherosclerotic plaques typically form in the areas of low wall shear stress (WSS) [7,8]. Endothelial cells activate inflammatory pathways under low WSS

* Corresponding author. Department of Biomechanical Engineering, Delft University of Technology, Mekelweg 5, Office: 34.E-1-340, Delft, 2628 CD, the Netherlands.
E-mail addresses: a.akyildiz@erasmusmc.nl, a.c.akyildiz@tudelft.nl (A.C. Akyildiz).

https://doi.org/10.1016/j.atherosclerosis.2025.120415
Received 16 January 2025; Received in revised form 7 May 2025; Accepted 24 June 2025
Available online 26 June 2025

conditions, leading to plaque initiation and development [9,10]. Also, high levels of the oscillatory shear index (OSI), which quantifies the oscillations (changes) in WSS, have been linked to plaque growth and destabilization of plaques [10,11].

The other class of vascular biomechanical factors is the blood pressure-driven ones (e.g., mechanical wall stress (MWS)) [12,13]. Although vascular cells, like endothelial and smooth muscle cells are mechanosensitive [14,15], the potential involvement of blood pressure-driven biomechanical factors in atherosclerosis has been mainly overlooked. For coronary arteries, we recently showed that the WSS and MWS, separately and combined, were associated with vessel wall and plaque composition change over time [16].

In this study, we investigate the impact of the pressure-driven biomechanical factors, individually and combined with flow-driven factors on carotid atherosclerosis, using artery-specific computational models and longitudinal carotid multidetector computational tomography angiography (MDCTA) scans.

2. Methods

2.1. Study design

The present study included participants (n = 244), from the Plaque At RISK cohort (PARISK) [16]. Participants in the PARISK study experienced recent (<3 months) large artery ischemic event, such as transient ischemic attack (TIA), minor stroke or amaurosis fugax, and had an ipsilateral carotid plaque of at least 2 mm thick with mild-to-moderate carotid artery stenosis (<70 %) at the time of study enrollment. A likely cause of a heart embolism (such as atrial fibrillation), renal clearance less than 30 mL/min, coagulation disorders, severe comorbidities and known allergies to contrast agents were among the exclusion criteria.

The baseline and 2-year follow-up MDCTA imaging was scheduled for 118 patients, but due to logistical problems (n = 13), contraindications for contrast material (n = 11), informed consent withdrawal (n = 9) and patient death (n = 3), the MDCTA scans were present for 82 patients. Information on cardiovascular risk factors (CVRF), comprising body mass index, hypertension, smoking status, hypercholesterolemia, diabetes mellitus and patients' medication was obtained at the baseline (Supplementary Data). Written informed permission was provided by each patient, and Institutional Ethical Review Board (IRB) authorisation (MEC 09-2-082) was acquired. The research centres' ethics committees had previously authorised the study procedure, which complied with the 1975 Declaration of Helsinki's ethical standards. Comprehensive details regarding the study's population have been published [17]. The reporting of this study adheres to the STROBE guidelines (Supplementary Data).

2.2. Data acquisition

A MDCT system was utilised to obtain the baseline and follow-up MDCTA records for the current investigation utilising an MDCTA technique with contrast enhancement. The cerebral circulation (3 cm above the sella turcica) and the ascending aorta were both included in the scan range. At an injection rate of 4 or 5 mL per second, each patient received 80–85 mL of an iodinated contrast agent (300–320 mg/mL) and a 45 mL saline bolus chaser. Detailed description of the imaging protocol has been previously published [17].

2.3. Artery segmentation and 3D reconstruction

Semi-automatic segmentation of the lumen, vessel wall, calcification, and lipid-rich necrotic core (LRNC) in the carotid bifurcations, on both sides, at baseline and follow-up (Fig. 1) was performed utilising the QAngioCT, Medis (version 3.2.0.13) [18,19]. A minimum of 30 horizontal CTA slices upstream and downstream of the carotid bifurcation were chosen in order to identify the region of interest (ROI). Then, QAngioCT performed longitudinal contouring, based on Hounsfield Units (HU), of the inner lumen (320–500 HU) and outer vessel wall (>90 HU) automatically [20,21], and manual adjustments were made as needed. To separate the calcium deposits from the contrast agent, the HU for the calcification detection was set higher than 600 HU [22,23] (Fig. 1). For LRNC detection, a HU range between −20 and 60 HU was used as reported before [24]. To assess intra- and inter-observer variability, the reader (A.T.) and a second trained reader (F.F.) independently re-segmented and evaluated a subset of 30 patients at both baseline and follow-up (120 arteries in total).

The baseline and follow-up 2D contours of the lumen, vessel wall, and plaque components were exported from QAngioCT 3D Workbench and converted into 3D solid surfaces (Fig. 1), using an in-house built MATLAB code (v.2017B, MathWorks). For each patient, the 3D artery geometries at baseline and follow-up were co-registered and aligned both longitudinally and circumferentially. This alignment was achieved using the location of the lumen flow divider at the carotid bifurcation

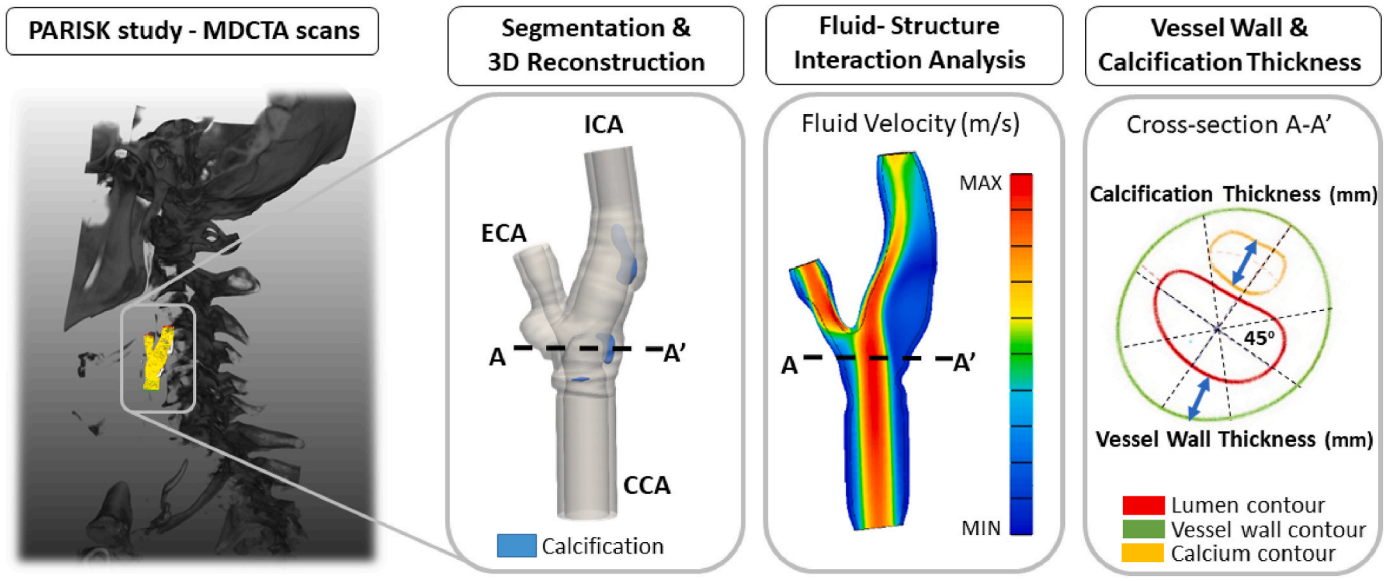

Fig. 1. Study design pipeline.

[25], the positions of the internal and external carotid arteries, and the reconstructed lumen centerlines [26], all processed by the in-house developed MATLAB code. Between the baseline and follow-up scans, the slice distance remained constant.

2.4. Computational modeling at baseline

The fluid-structure Interaction (FSI) modeling approach was used to compute the pressure-driven and flow-driven biomechanical stress metrics at the carotid arteries [27]. In the FSI modeling approach, blood flow is simulated within the lumen of the carotid arteries, allowing the arterial wall to deform accordingly to account for the interaction between fluid flow and arterial wall deformation. Flow extensions to the inlet (CCA) and outlet (ICA & ECA) were added to the 3D reconstructed carotid arteries. Then, the geometries were uploaded into the FSI modeling software FEBio Studio (Columbia University, University of Utah, version 2.6), that has previously been utilised for FSI analysis in the carotid bifurcation [28,29]. A mesh sensitivity analysis was conducted to ensure that numerical simulation results were independent of the mesh resolution, using the Grid Convergence Index method [30], resulting in, approximately, $450{\cdot}10^3$ "tet4" elements and $150{\cdot}10^3$ "penta6" elements per artery.

The backward incremental approach [12] was utilised to ascertain the existing stresses within the carotid geometries via the prestrain method of FEBio. Specifically, we calculated the strain distribution within the carotid vessel wall at the moment the MDCTA scans were acquired and integrated this distribution into the FSI model as the "initial strain" of the artery. The material properties of the plaque components were modeled as isotropic, nonlinear, hyperelastic, and incompressible, using a modified Mooney-Rivlin model (Supplementary Data: Table S1) [4,12,31]. Blood was considered to be incompressible, non-Newtonian and modeled using the Carreau model with a no-slip and Fluid-FSI traction boundary condition implemented. According to a mean flow profile presented in Lee et al. study [32], a transient flow curve was implemented at CCA. The flow curve was adjusted so that the mean flow matched the patient-specific flow values in the CCA as determined by ultrasound Doppler. Color Doppler velocity data was combined with local arterial diameter measurements to determine the flow in order to reduce sensitivity to measurement artefacts. Additionally, a patient-specific heart rate that was obtained from ultrasound Doppler readings was used. In the CCA inlet, a parabolic flow curve was suggested, utilising these patient-specific flow profiles [33]. According the literature [34], the ICA and ECA were estimated to have outflow values of 64 % and 36 %, respectively. The boundary condition at outflow was applied by using the distal vascular resistance model [35]. The simulation was completed for two heart cycles. The biomechanical stress parameters were calculated in the second cardiac cycle, while initialization was done in the first. Every cardiac cycle was split up into 100 time increments.

2.5. Biomechanical factors

Across the entire length of the carotid artery, the following pressure-driven biomechanical factors were calculated: the maximum and time-averaged (i.e., averaged over a cardiac cycle) von Mises and max Principal stresses were calculated at the lumen and within the vessel wall. Regarding the flow-driven biomechanical factors, the following metrics were calculated: the cross-flow index (CFI), which quantifies the extent of secondary or transverse flow components over the arterial wall; the oscillatory shear index (OSI), which represents the ratio of backward to forward shear stress; the relative residence time (RRT), indicating the duration blood remains at a specific arterial site; the time-averaged wall shear stress (TAWSS), which measures the average wall shear stress over a cardiac cycle; and transverse wall shear stress (transWSS), which describes the shear stress acting perpendicular to the primary flow direction along the vessel's surface [11,36]. A detailed definition of the biomechanical factors is provided in Supplementary Data: Table S2.

2.6. Change in vessel wall thickness and structure

The radial length between the lumen and the outer vessel wall was determined in order to calculate the vessel wall thickness change (ΔWT) in cross-sections orthogonal to the centerline, by subtracting the baseline measurements from the 2-year follow-up measurements. The alterations in arterial structure, on both baseline and follow-up, were evaluated by the absolute and relative thickness change of calcifications, and by the change of the radial distance between the lumen surface and calcification.

2.7. Statistical analysis

Continuous variables are presented as mean with standard deviation or in case of skewed distribution, as median with interquartile range [Q1-Q3], and the categorical variables as absolute numbers with relative frequencies. The intra- and inter-observer variability was estimated via the intraclass correlation (Bland-Altman plots) of lumen, vessel wall, plaque burden (i.e., the plaque volume in the total arterial area (%)), and calcification cross-sectional area measurements. We determined the correlations between the pressure-driven and flow-driven biomechanical stress metrics, using Spearman correlation tests and calculated the distributions of the metrics at baseline and follow-up.

Every artery was separated into sectors that were 1 mm long (longitudinally) and 45° wide (circumferentially). The external carotid artery (ECA) and the inflow and outflow extensions were excluded from further analyses. The sectors were split, based on 1.5 mm thickness, into sectors free of plaque or plaque-containing. ΔWT, compositional changes, and all pressure-driven and flow-driven biomechanical factors were quantified per sector, and the biomechanical factors were split into tertiles (low, mid, and high).

The mixed model effect was applied to investigate the association between baseline biomechanical stress metrics in plaque sectors with the vessel wall thickness and plaque composition at follow-up in carotid arteries and specifically, the generalized linear mixed model (GLMM) was implemented. The pressure-driven and flow-driven biomechanical stress metrics, the calcification presence, the interaction between pressure-driven and flow-driven biomechanics, the interaction between pressure-driven biomechanics and calcification presence, and the interaction between flow-driven biomechanics and calcification presence were used as fixed factors. Repeated comparisons of the p-values were corrected using the Bonferroni technique. The artery and patient information was used as random factors to acknowledge the intra-artery and within-patient correlations while correcting for patient age, sex, and cardiovascular risk factors including smoking, diabetes, obesity, hypertension, hypercholesterolemia and patients' medication at baseline. A two-tailed $p < 0.05$ was chosen as the significance level, using SPSS (IBM 27). The follow-up analysis was adjusted for baseline metrics to reflect the change over time. Deducting the adjusted baseline metrics from the estimated follow-up metrics provided the ΔWT and the compositional changes.

3. Results

3.1. Patient and sector characteristics

Fig. 2 illustrates the study design flowchart for patient inclusion. Out of the 82 patients from the PARISK cohort who underwent MDCTA imaging at baseline and at the 2-year follow-up, seven were excluded from the prospective analysis—two due to poor-quality CTA scans and five due to missing ultrasound color Doppler measurements. The remaining 75 patients were included in the current study.

In Table 1 the population's characteristics at the time of inclusion are listed. In brief, the study group (n = 75) presented a mean age of 66 ±

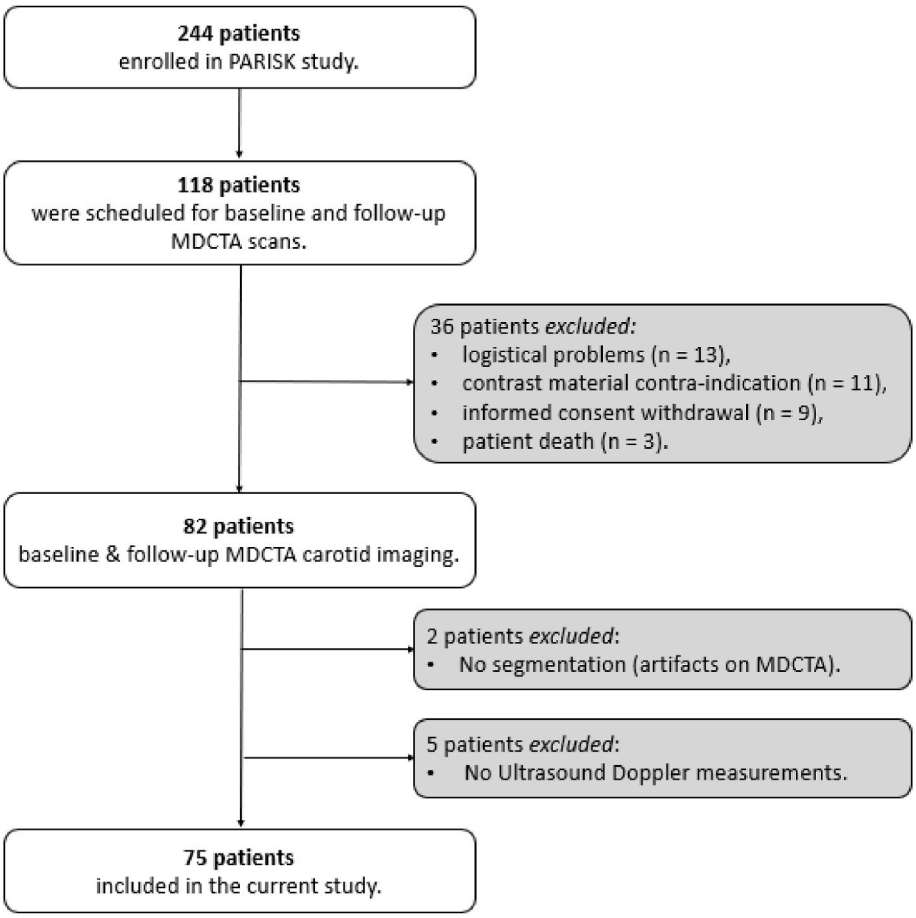

Fig. 2. Study design flowchart.

Table 1
Patients' characteristics at time of study inclusion.

Patients' characteristics at time of study inclusion (n = 75)	
Age (years, mean ± SD):	66 ± 8.3
Sex (men, n (%)):	56 (75 %)
BMI (kg/m^2, mean ± SD):	26 ± 4.1
Hypertension, n (%):	58 (77 %)
Hypercholesterolemia, n (%):	59 (78 %)
Diabetes Mellitus, n (%):	14 (19 %)
Current Smoking, n (%):	24 (32 %)
Medication use at index event:	
Use of statins, n (%)	36 (48 %)
Use of antihypertensive drugs, n (%)	40 (53 %)
Use of antithrombotic drugs, n (%)	29 (39 %)

SD: standard deviation.

8.3 years, 19 % had diabetes mellitus, 77 % had hypertension, 78 % had hypercholesterolemia, and 32 % were current smokers. The group was predominantly male (75 %), with no significant variations in cardiovascular risk factor distribution between men and women. Patients who were on statin therapy before baseline or started statin treatment after baseline did not show significant differences in vessel wall or calcification thickness at follow-up. During the follow-up period, seven patients quit smoking, while the distribution of other cardiovascular risk factors remained similar.

From the 150 carotid arteries imaged (75 patients), 33637 sectors were obtained and analyzed. At baseline, 23 % (n = 7819) of the sectors had plaque (55 % (n = 4301) of these sections included calcifications and 2 % (n = 167) presented soft plaque components). At follow-up, 5682 sectors showed calcifications and 298 sectors contained soft plaque components. At the time of inclusion, sectors with plaque presented 2.1 mm median WT (1.7–2.5 mm). Both calcified and non-calcified sectors displayed baseline WT of 2.4 mm (1.9–2.9 mm) and 1.7 mm (1.6–2.1 mm), respectively. In plaque sectors with calcifications, the absolute and relative median (range) of calcification thickness was 0.6 mm (0.2–1.2 mm) and 21 % (7–40 %), respectively. The lumen-calcification distance at baseline showed a median (range) of 0.2 mm (0.1–0.4 mm).

Excellent agreement was found in the assessment of intra- and inter-observer variability; a detailed analysis is provided in Supplementary Data Table S3 and Fig. S1. The pressure-driven and flow-driven stress metrics at baseline were not correlated ($r \ll 0.7$) (Supplementary Table S4). However, all (pressure-driven) mechanical wall stress metrics were highly correlated ($r > 0.9$) and showed similar stress distribution patterns. As a result, only max principal stress in the lumen (MWS) was used for further statistical analyses. For the (flow-driven) shear stress metrics, the TAWSS, CFI, OSI, and transWSS were uncorrelated ($r < 0.75$) and were included in the further statistical analyses.

For pressure-driven stress metrics, the tertiles were separated based on 42.7 kPa and 63.6 kPa, for TAWSS tertiles the 0.7 Pa and 1.9 Pa values were used, for CFI tertiles 0.03 and 0.07 values were applied, for OSI tertiles 0.004 and 0.03 numbers were set and for transWSS tertiles 0.06 Pa and 0.15 Pa values were applied.

3.2. Biomechanics and plaque thickness change

During the two-year study period, plaque sectors presented a median ΔWT (i.e., baseline measurements were subtracted from the 2-year follow-up measurements) of 0.01 mm, IQR [−0.2, 0.2] and 55 % of sectors presented a reduction in wall thickness. The Supplementary

Table S5 offers more thorough baseline and follow-up WT measures. Only baseline MWS and the interaction term of the baseline MWS and OSI were statistically significant for ΔWT, whereas baseline OSI alone showed no significant association with ΔWT. A negative association between MWS and ΔWT ($p < 0.001$) was found where higher levels of MWS were associated with a greater decrease in wall thickness (Fig. 3A). The interaction effect of MWS and OSI revealed that the combination of high MWS and low OSI was associated ($p < 0.05$) with the highest decrease in wall thickness over time (Fig. 3B).

The plaque sectors were further stratified based on the calcification presence at baseline. Calcified plaque sectors (55 % of plaque sectors) presented a median ΔWT of 0.04 mm, IQR [−0.2, 0.2], compared to non-calcified sectors with a median ΔWT of - 0.01 mm, IQR [−0.2, 0.2] (Supplementary Table S5). The ΔWT was significantly different ($p < 0.001$) between plaque sectors with and without calcification (Fig. 3C). The baseline MWS distribution was also significantly different ($p < 0.001$) between plaque sectors with and without calcification, where the ΔWT was associated with the baseline MWS only in non-calcified plaque sectors (Fig. 3D).

3.3. Biomechanics and calcium thickness change

Plaque sectors with calcification at baseline revealed a median calcification thickness change of 0.04 mm, IQR [−0.1, 0.4] (relative thickness change of 2 %, IQR [−6, 12]. During the two-year study period, 65 % of the calcified sectors demonstrated an increase in calcification thickness. The Supplementary Table S6 and Table S7 offer more thorough absolute and relative calcification thickness measures. The baseline MWS was significantly associated ($p < 0.001$) with the absolute and relative calcification thickness change over time, where the lower baseline MWS correlated with higher calcification thickness increase over time (Fig. 4A). The opposite trend ($p < 0.05$) was found between the baseline OSI and the calcification thickness change, revealing that higher levels of OSI were associated with a greater increase in calcification thickness over time (Fig. 4B).

3.4. Biomechanics and lumen - calcium distance change

Calcified plaque sectors presented a median lumen - calcification distance change of −0.02 mm, IQR [−0.2, 0.1] and 69 % of these sectors presented a reduction in lumen - calcification distance over time. The lumen – calcification distance parameters at baseline and follow-up are explained in the Supplementary Table S8. Baseline TAWSS was significantly associated with changes in the lumen-calcification distance over time ($p < 0.01$), with higher baseline TAWSS correlating with a greater reduction in lumen-calcification distance (Fig. 4C). A similar trend was observed for baseline MWS ($p < 0.05$), showing that higher MWS levels were associated with a more pronounced decrease in calcification thickness over time (Fig. 4D). Regarding the association of baseline MWS with the outer vessel wall – calcification distance change over time, a significant positive ($p < 0.01$) trend was observed (Supplementary Fig. S2).

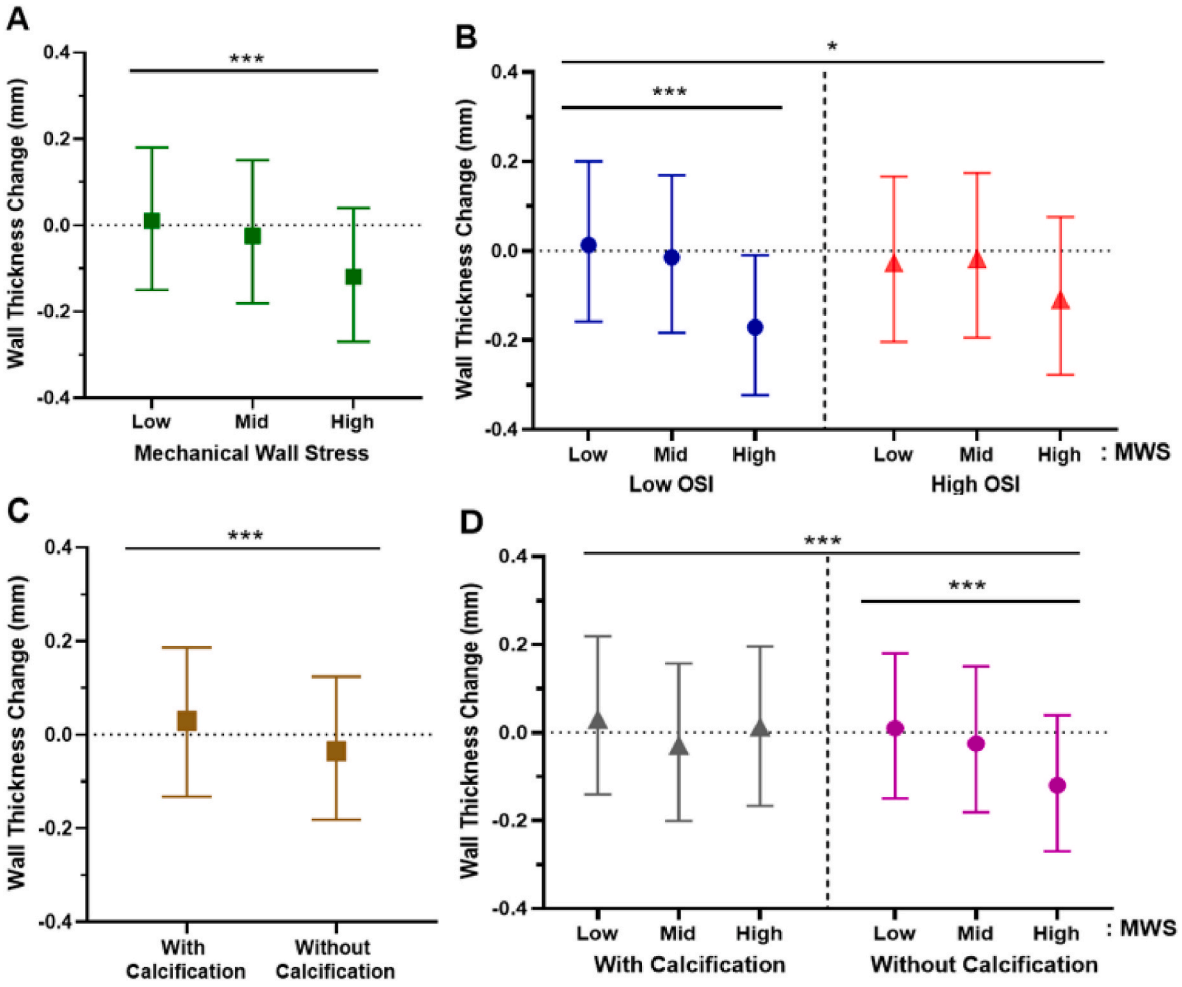

Fig. 3. (A) Association of baseline MWS with wall thickness change, (B) association of combination of baseline MWS and OSI with wall thickness change, (C) association of calcification presence in plaque sectors with wall thickness change, (D) association of baseline MWS, stratified by calcification presence, with wall thickness change, in plaque sectors based on GLMM (mean, 95 % CI), CI: confidence interval; ***: $p < 0.001$; **: $p < 0.01$; *: $p < 0.05$.

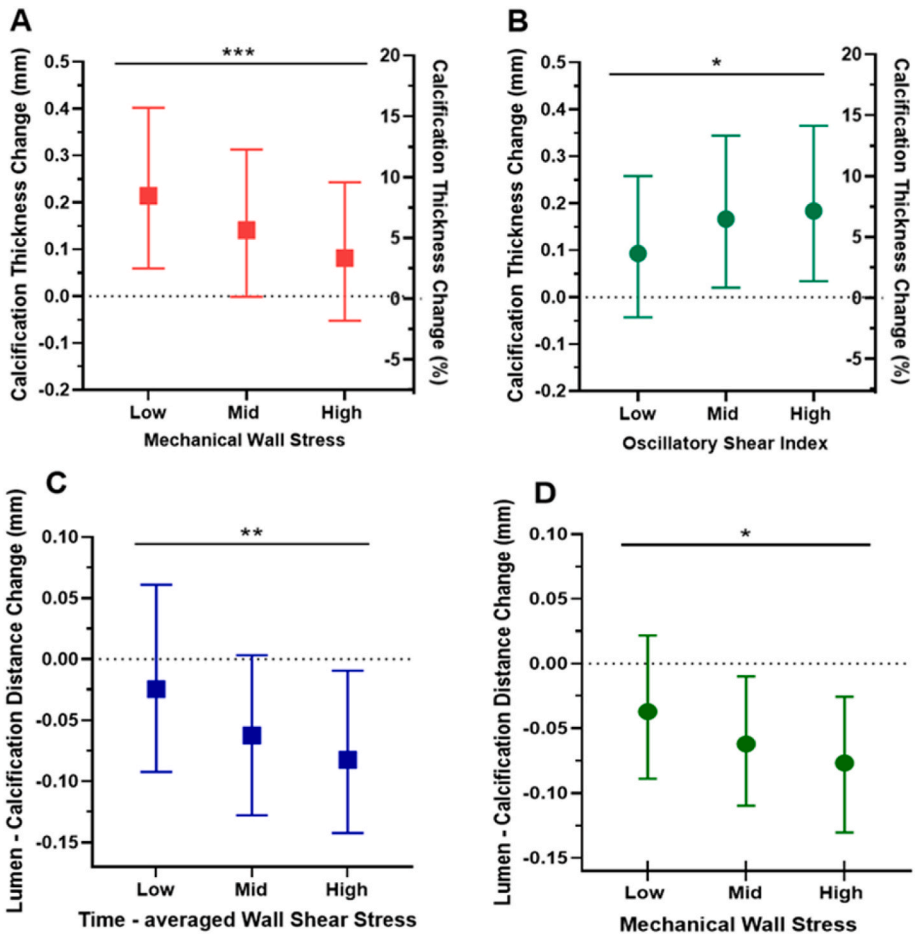

Fig. 4. (A) Association of baseline mechanical wall stress with calcification absolute and relative thickness change, (B) association of baseline oscillatory shear index with calcification absolute and relative thickness change, (C) association of baseline time-averaged wall shear stress with lumen-calcification distance change, (D) association of baseline mechanical wall stress with lumen-calcification distance change, in plaque sectors based on GLMM (mean, 95 % CI), CI: confidence interval; ***: $p < 0.001$; **: $p < 0.01$; *: $p < 0.05$.

4. Discussion

The influence of the individual and combined effect of pressure-driven and flow-driven biomechanical factors on the development of carotid artery disease was assessed in this study. Our main findings regarding the carotid plaque sectors are summarized as follows: (1) high MWS (combined with low OSI) is associated with greater vessel wall reduction over time, (2) low MWS and high OSI are associated with greater calcification thickness increase, and (3) high TAWSS and high MWS are associated with higher lumen - calcification distance decrease over time.

The measurements of our study showed that, at the baseline, half of the plaque sectors contained calcification. Calcification is a highly prevalent structural component in atherosclerotic carotid arteries [2]. Over the two-year follow-up time of our study, we observed that the plaque sectors, with calcified and non-calcified sectors combined, exhibited minimal change in wall thickness. However, in calcified plaque sectors, the calcification thickness increased. The impact of statin medication may be the cause of these results. It is well established that statins prevent plaque progression while, paradoxically, promote calcification progression [37,38]. In addition, the distance between lumen and calcification decreased over time, highlighting the active remodeling process of carotid calcifications within plaques [39,40].

Our analysis is the first to present the influence of pressure-driven biomechanical factors, combined with flow-driven ones, on carotid atherosclerosis. In agreement with our previous research on human coronaries [16], our analyses demonstrated that high MWS also correlates with greater plaque thickness reduction in non-calcified regions of plaques in carotid arteries. Similarly, in human coronary arteries, the reduction of fibrous tissue was linked to increased MWS, as reported by Costopoulos et al. [4]. Moreover, the co-existence of low OSI, reflecting a more stable, unidirectional, atheroprotective blood flow [41], with high MWS, highlighted their interactive effect on atherosclerosis by causing the greatest decrease in plaque thickness in carotid arteries.

Previous studies [8,11,42] have shown that high OSI (i.e., disturbed flow patterns) contributes to adverse hemodynamic conditions that promote endothelial dysfunction and inflammatory pathways, leading to abnormal tissue remodeling, which could potentially be a precursor to calcification development. Mirza et al. [43] and Hsu et al. [44] presented the association of high OSI values with the development of calcific aortic valve disease (CAVD), suggesting a link between disturbed blood flow patterns and calcification development. Our results not only support this finding but also demonstrate that also low MWS is associated with greater calcification thickness increase over time. Earlier research [45,46] indicated that lower MWS was correlated with more stable plaque characteristics, which may promote calcification growth over time. However, high MWS showed an ambiguous influence on calcification thickness change. When considering the associations with wall thickness change observed in our study, high MWS had minimal or no effect on calcified sectors or on calcification thickness change over time. Furthermore, high levels of WSS or MWS are known to be associated with vascular remodeling [16,47]. In line with that, our study demonstrated that high TAWSS and high MWS are related

independently to a greater reduction in the distance between the lumen and calcification.

Our study has several limitations. First, we only segmented calcifications with densities exceeding 600 HU [22], which may have resulted in the low-density calcifications being overlooked and an underestimation of the total calcification volume. Second, the patients either were already at the study enrollment or were put during the study under statin treatment. Therefore, the potential impact of statins on carotid atherosclerosis [38] should be taken into account when interpreting our study findings. Third, our study focused specifically on carotid calcifications, for which standard clinical CTA scans were sufficient for accurate detection and segmentation. Emerging advancements in CT imaging, such as photon-counting computed tomography [48], may further enhance the assessment of soft plaque components and their interaction with calcifications.

5. Conclusion

The association of pressure-driven and flow-driven biomechanical factors, individually and combined, with atherosclerosis development in carotid arteries was examined. Our analyses demonstrated that high MWS (combined with low OSI) was correlated with greater plaque thickness reduction over time, high MWS and low OSI were independently associated with greater calcification thickness increase, and high TAWSS and high MWS were associated with higher lumen - calcification distance decrease over time. Our findings provide new insights into carotid artery disease and the role of biomechanical factors in its development.

CRediT authorship contribution statement

Aikaterini Tziotziou: data analysis, software development, Writing – original draft. **Yanjing Liu:** software development, Writing – review & editing. **Federica Fontana:** data analysis, Writing – review & editing. **Juul Bierens:** data collection, Writing – review & editing. **Paul J. Nederkoorn:** data collection, Writing – review & editing. **Pim A. de Jong:** data collection, Writing – review & editing. **M. Eline Kooi:** data collection, Writing – review & editing. **Werner Mess:** data collection, Writing – review & editing. **Aad van der Lugt:** Supervision, Writing – review & editing. **Antonius F.W. van der Steen:** Supervision, Writing – review & editing. **Daniel Bos:** Supervision, Conceptualization, Writing – review & editing. **Jolanda J. Wentzel:** Conceptualization, Writing – review & editing. **Ali C. Akyildiz:** Supervision, Conceptualization, Writing – review & editing.

Ethical approval

Medical Ethics Committee authorised the study (1975 Declaration of Helsinki ethical standards, MEC 09-2-082, clinical trials.gov NCT01208025).

Data availability

The data supporting this article cannot be shared publicly due to the privacy of individuals who participated in the study. The data can be made available by the corresponding author upon reasonable request.

Financial support

This research is part of a project that has received funding from the European Research Council (ERC) under Horizon 2020 research and innovation program (Grant agreement No. 101042724 — MicroMechAthero) and performed within the framework of the European Research Council (ERC) (www.ctmm.nl), project PARISK (Plaque At RISK; grant number 01C-202).

Aikaterini Tziotziou was supported by Erasmus MC MRace grant PhD project.

Declaration of competing interest

The authors declare that they have no known competing financial interests or personal relationships that could have appeared to influence the work reported in this paper.

Acknowledgments

We thank the study participants and the clinical staff for their dedication and involvement to the Plaque At Risk (PARISK) Study.

Appendix A. Supplementary data

Supplementary data to this article can be found online at https://doi.org/10.1016/j.atherosclerosis.2025.120415.

References

[1] Bonati LH, Kakkos S, Berkefeld J, et al. European stroke organization guideline on endarterectomy and stenting for carotid artery stenosis. Eur Stroke J 2021;6:1–47. https://doi.org/10.1177/23969873211026990.
[2] Bos D, Arshi B, van den Bouwhuijsen QJA, et al. Atherosclerotic carotid plaque composition and incident stroke and coronary events. J Am Coll Cardiol 2021;77(11):1426–35. https://doi.org/10.1016/j.jacc.2021.01.038.
[3] van Dam-Nolen DHK, van Egmond NCM, Koudstaal PJ, et al. Sex differences in carotid atherosclerosis: a systematic review and meta-analysis. Stroke 2023;54(2):315–26. https://doi.org/10.1161/STROKEAHA.122.041046.
[4] Costopoulos C, Timmins LH, Huang Y, et al. Impact of combined plaque structural stress and wall shear stress on coronary plaque progression, regression, and changes in composition. Eur Heart J 2019;40:1411–22. https://doi.org/10.1093/eurheartj/ehz132.
[5] Conway DE, Schwartz MA. Flow-dependent cellular mechanotransduction in atherosclerosis. J Cell Sci 2013;126:5101–9. https://doi.org/10.1242/jcs.138313.
[6] Chatzizisis YS, Jonas M, Coskun AU, et al. Prediction of the localization of high-risk coronary atherosclerotic plaques on the basis of low endothelial shear stress-an intravascular ultrasound and histopathology natural history study. Circulation 2008;117:993–1002.
[7] Ku DN, Giddens DP, Zarins CK, et al. Pulsatile flow and atherosclerosis in the human carotid bifurcation. Positive correlation between plaque location and low oscillating shear stress. Arteriosclerosis 1985;5:293–302. https://doi.org/10.1161/01.ATV.5.3.293.
[8] Peiffer V, Sherwin SJ, Weinberg Pd PD. Does low and oscillatory wall shear stress correlate spatially with early atherosclerosis? A systematic review. Cardiovasc Res 2013;99:242–50. https://doi.org/10.1093/cvr/cvt044.
[9] Stone PH, Maehara A, Coskun AU, et al. Role of low endothelial shear stress and plaque characteristics in the prediction of nonculprit major adverse cardiac events: the PROSPECT study. JACC Cardiovasc Imaging 2018;11:462–71.
[10] Wentzel JJ, Chatzizisis YS, Gijsen FJH, et al. Endothelial shear stress in the evolution of coronary atherosclerotic plaque and vascular remodelling: current understanding and remaining questions. Cardiovasc Res 2012;96:234–43.
[11] Rikhtegar F, Knight JA, Olgac U, et al. Choosing the optimal wall shear parameter for the prediction of plaque location-A patient-specific computational study in human left coronary arteries. Atherosclerosis 2012;221:432–7. https://doi.org/10.1016/j.atherosclerosis.2012.01.018.
[12] Akyildiz AC, Speelman L, Nieuwstadt HA, et al. The effects of plaque morphology and material properties on peak cap stress in human coronary arteries. Comput Methods Biomech Biomed Eng 2016;19:771–9. https://doi.org/10.1080/10255842.2015.1062091.
[13] Akyildiz AC, Speelman L, van Brummelen H, et al. Effects of intima stiffness and plaque morphology on peak cap stress. Biomed Eng Online 2011;10:25. https://doi.org/10.1186/1475-925X-10-25.
[14] Hirata K, Ishida T, Matsushita H, et al. Regulated expression of endothelial cell derived lipase. Biochem Biophys Res Commun 2000;272:90–3. https://doi.org/10.1006/bbrc.2000.2747.
[15] Humphrey JD, Harrison DG, Figueroa CA, et al. Central artery stiffness in hypertension and aging. Circ Res 2016;118:379–81. https://doi.org/10.1161/CIRCRESAHA.115.307722.
[16] Tziotziou A, Hartman E, Korteland SA, et al. Mechanical wall stress and wall shear stress are associated with atherosclerosis development in non-calcified coronary segments. Atherosclerosis 2023;387:117387. https://doi.org/10.1016/j.atherosclerosis.2023.117387.
[17] Truijman MTB, Kooi ME, van Dijk AC, et al. Plaque at RISK (PARISK): prospective multicenter study to improve diagnosis of high-risk carotid plaques. Int J Stroke 2014;9:747–54. https://doi.org/10.1111/ijs.12167.
[18] Lansky A, Tuinenburg J, Costa M, et al. Quantitative angiographic methods for bifurcation lesions: a consensus statement from the european bifurcation group. Cathet Cardiovasc Interv 2009;73(2):258–66. https://doi.org/10.1002/ccd.21814.

[19] Ishibashi Y, Grundeken MJ, Nakatani S, et al. In vitro validation and comparison of different software packages or algorithms for coronary bifurcation analysis using calibrated phantoms: implications for clinical practice and research of bifurcation stenting. Cathet Cardiovasc Interv 2015;85(4):554–63. https://doi.org/10.1002/ccd.25618.
[20] Williams MC, Earls JP, Hecht H. Quantitative assessment of atherosclerotic plaque, recent progress, and current limitations. J Cardiovasc Comput Tomogr 2022;16:124–37. https://doi.org/10.1016/j.jcct.2021.07.001.
[21] de Graaf MA, Broersen A, Kitslaar PH, et al. Automatic quantification and characterization of coronary atherosclerosis with computed tomography coronary angiography: cross-correlation with intravascular ultrasound virtual histology. Int J Cardiovasc Imag 2013;29:1177–90. https://doi.org/10.1007/s10554-013-0194-x.
[22] Glodny B, Helmel B, Trieb T, et al. A method for calcium quantification by means of CT coronary angiography using 64-multidetector CT: very high correlation with Agatston and volume scores. Eur Radiol 2009;19:1661–8. https://doi.org/10.1007/s00330-009-1345-2.
[23] van Dam-Nolen D, van Dijk AC, Crombag G, et al. Lipoprotein(a) levels and atherosclerotic plaque characteristics in the carotid artery: the Plaque at RISK (PARISK) study. Atherosclerosis 2021;329:22–9. https://doi.org/10.1016/j.atherosclerosis.2021.06.004.
[24] de Weert TT, Ouhlous M, Meijering E, et al. In vivo characterization and quantification of atherosclerotic carotid plaque components with multidetector computed tomography and histopathological correlation. Arterioscler Thromb Vasc Biol 2006;26(10):2366–72. https://doi.org/10.1161/01.ATV.0000240518.90124.57.
[25] Groen HC, Gijsen FJ, van der Lugt A, et al. Plaque rupture in the carotid artery is localized at the high shear stress region: a case report. Stroke 2007;38(8):2379–81. https://doi.org/10.1161/STROKEAHA.107.484766.
[26] Wang Q, Tang D, Wang L, et al. Combining morphological and biomechanical factors for optimal carotid plaque progression prediction: an MRI-based follow-up study using 3D thin-layer models. Int J Cardiol 2019;15:266–71. https://doi.org/10.1016/j.ijcard.2019.07.005.
[27] Bantwal A, Singh A, Ramachandran Menon A, et al. Pathogenesis of atherosclerosis and its influence on local hemodynamics: a comparative FSI study in healthy and mildly stenosed carotid arteries. Int J Eng Sci 2021;167:103525. https://doi.org/10.1016/j.ijengsci.2021.103525.
[28] Shim JJ, Maas SA, Weiss JA, Ateshian GA. A formulation for fluid-structure interactions in febio using mixture theory. J Biomech Eng 2019;141:510101–5101015. https://doi.org/10.1115/1.4043031.
[29] Shim JJ, Maas SA, Weiss JA, Ateshian GA. Finite element implementation of biphasic-fluid structure interactions in febio. J Biomech Eng 2021;143:091005. https://doi.org/10.1115/1.4050646.
[30] Roache PJ. Verification of codes and calculations. AIAA J 1998;36:5.
[31] Guvenir Torun S, Torun HM, Hansen HHG, et al. Multicomponent material property characterization of atherosclerotic human carotid arteries through a Bayesian optimization based inverse finite element approach. J Mech Behav Biomed Mater 2022;126:104996. https://doi.org/10.1016/j.jmbbm.2021.104996.
[32] Lee SW, Antiga L, Spence JD, Steinman DA. Geometry of the carotid bifurcation predicts its exposure to disturbed flow. Stroke 2008;39:2341–7. https://doi.org/10.1161/STROKEAHA.107.510644.
[33] Womersley JR. Method for the calculation of velocity, rate of flow and viscous drag in arteries when the pressure gradient is known. J Physiol 1955;127:553–63. https://doi.org/10.1113/jphysiol.1955.sp005276.
[34] Groen HC, Simons L, van den Bouwhuijsen QJA, et al. MRI-based quantification of outflow boundary conditions for computational fluid dynamics of stenosed human carotid arteries. J Biomech 2010;43:2332–8. https://doi.org/10.1016/j.jbiomech.2010.04.039.
[35] Lee SH, Kang S, Hur N. An approach on fluid-structure interaction for hemodynamics of carotid arteries, in fluids engineering division summer meeting. Am Soc Mech Eng 2012;44762:253–7.
[36] Hoogendoorn A, Kok AM, Hartman EMJ, et al. Multidirectional wall shear stress promotes advanced coronary plaque development: comparing five shear stress metrics. Cardiovasc Res 2020;116(6):1136–46. https://doi.org/10.1093/cvr/cvz212.
[37] Bittencourt MS, Cerci RJ. Statin effects on atherosclerotic plaques: regression or healing? BMC Med 2015;13:260. https://doi.org/10.1186/s12916-015-0499-9.
[38] Achenbach S, Ropers D, Pohle K, et al. Influence of lipid-lowering therapy on the progression of coronary artery calcification: a prospective evaluation. Circulation 2002;106(9):1077–82. https://doi.org/10.1161/01.cir.0000027567.49283.ff.
[39] Xu S, Zhang J, Yang J, et al. Evaluating the association between vascular remodeling and plaque calcification patterns of the carotid artery and its effects on ischemic symptoms using CT angiography. Cardiovasc Diagn Ther 2024;14(2):229–39. https://doi.org/10.21037/cdt-23-428.
[40] Tian J, Gu X, Sun Y, et al. Effect of statin therapy on the progression of coronary atherosclerosis. BMC Cardiovasc Disord 2012;1:12:70. https://doi.org/10.1186/1471-2261-12-70.
[41] Kumar N, Pai R, Abdul Khader SM, et al. Influence of blood pressure and rheology on oscillatory shear index and wall shear stress in the carotid artery. J Braz Soc Mech Sci Eng 2022;44:510. https://doi.org/10.1007/s40430-022-03792-5.
[42] Dong M, Chen M, Zhang Y, et al. Oscillatory shear stress promotes endothelial senescence and atherosclerosis via STING activation. Biochem Biophys Res Commun 2024;715:149979. https://doi.org/10.1016/j.bbrc.2024.149979.
[43] Mirza A, Hsu CPD, Rodriguez A, et al. Computational model for early-stage aortic valve calcification shows hemodynamic biomarkers. Bioengineering 2024;11:955. https://doi.org/10.3390/bioengineering11100955.
[44] Hsu CPD, Tchir A, Mirza A, et al. Valve endothelial cell exposure to high levels of flow oscillations exacerbates valve interstitial cell calcification. Bioengineering 2022;9:393. https://doi.org/10.3390/bioengineering9080393.
[45] Wong KK, Thavornpattanapong P, Cheung SC, et al. Effect of calcification on the mechanical stability of plaque based on a three-dimensional carotid bifurcation model. BMC Cardiovasc Disord 2012;12:7. https://doi.org/10.1186/1471-2261-12-7.
[46] Dayawansa NH, Baratchi S, Peter K. Uncoupling the vicious cycle of mechanical stress and inflammation in calcific aortic valve disease. Front Cardiovasc Med 2022;9:783543. https://doi.org/10.3389/fcvm.2022.783543.
[47] Dolan JM, Kolega J, Meng H. High wall shear stress and spatial gradients in vascular pathology: a review. Ann Biomed Eng 2013;41(7):1411–27. https://doi.org/10.1007/s10439-012-0695-0.
[48] Van der Bie J, van Straten M, Booij R, et al. Photon-counting CT: review of initial clinical results. Eur J Radiol 2013;163:110829. https://doi.org/10.1016/j.ejrad.2023.110829.